Journal of Neuroscience Methods 350 (2021) 109039

Contents lists available at ScienceDirect

Journal of Neuroscience Methods

journal homepage: www.elsevier.com/locate/jneumeth

Graph-theoretical analysis identifies transient spatial states of resting-state dynamic functional network connectivity and reveals dysconnectivity in schizophrenia

Qunfang Long [a,*,1], Suchita Bhinge [a], Vince D. Calhoun [b,c,d], Tülay Adali [a]

[a] Department of Computer Science and Electrical Engineering, University of Maryland Baltimore County, Baltimore, MD, 21250, USA
[b] The Mind Research Network, Albuquerque, NM, 87131, USA
[c] Department of Electrical and Computer Engineering, University of New Mexico, Albuquerque, NM, 87131, USA
[d] Tri-institutional Center for Translational Research in Neuroimaging and Data Science (TReNDS), Georgia State University, Georgia Institute of Technology, Emory University, Atlanta, GA, USA

ARTICLE INFO

Keywords:
Dynamic functional network connectivity
Graph-theoretical analysis
Dynamic study
Adaptively constrained independent vector analysis
Functional magnetic resonance imaging

ABSTRACT

Background: Dynamic functional network connectivity (dFNC) summarizes associations among time-varying brain networks and is widely used for studying dynamics. However, most previous studies compute dFNC using temporal variability while spatial variability started receiving increasing attention. It is hence desirable to investigate spatial variability and the interaction between temporal and spatial variability.
New method: We propose to use an adaptive variant of constrained independent vector analysis to simultaneously capture temporal and spatial variability, and introduce a goal-driven scheme for addressing a key challenge in dFNC analysis—determining the number of transient states. We apply our methods to resting-state functional magnetic resonance imaging data of schizophrenia patients (SZs) and healthy controls (HCs).
Results: The results show spatial variability provides more features discriminative between groups than temporal variability. A comprehensive study of graph-theoretical (GT) metrics determines the optimal number of spatial states and suggests centrality as a key metric. Four networks yield significantly different levels of involvement in SZs and HCs. The high involvement of a component that relates to multiple distributed brain regions highlights dysconnectivity in SZ. One frontoparietal component and one frontal component demonstrate higher involvement in HCs, suggesting a more efficient cognitive control system relative to SZs.
Comparison with existing methods: Spatial variability is more informative than temporal variability. The proposed goal-driven scheme determines the optimal number of states in a more interpretable way by making use of discriminative features.
Conclusion: GT analysis is promising in dFNC analysis as it identifies distinctive transient spatial states of dFNC and reveals unique biomedical patterns in SZs.

1. Introduction

There is evidence that shows that the intrinsic functional patterns in the human brain change over time. These time-varying—dynamic—patterns can be studied using resting-state functional magnetic resonance imaging (fMRI) data (Chang and Glover, 2010; Hutchison et al., 2013a, b; He et al., 2018; Chen, 2019). Resting-state fMRI captures the blood-oxygenation-level-dependent (BOLD) response of neurons in the brain in the absence of external input or stimulus-evoked cognitive processing. Data-driven blind source separation techniques are widely used in fMRI analysis by assuming the observed data is a linear mixture of latent factors. A decomposition of resting-state fMRI data extracts resting-state networks (RSNs) that consists of cortical and subcortical areas with synchronized BOLD activities. Dynamic functional network connectivity (dFNC) or dynamic functional connectivity (dFC) that summarizes the association among BOLD activation patterns of RSNs or regions of interest (ROIs) has been a widely used feature for the study of brain dynamics (Jafri et al., 2008;

* Corresponding author.
E-mail address: qunfang1@umbc.edu (Q. Long).
[1] URL: http://mlsp.umbc.edu/.

https://doi.org/10.1016/j.jneumeth.2020.109039
Received 14 August 2020; Received in revised form 8 December 2020; Accepted 9 December 2020
Available online 25 December 2020

Wang et al., 2010; Calhoun et al., 2014; Kucyi and Davis, 2014; Park et al., 2018; Lee and Kim, 2019; Weber et al., 2020). Unique dFNC patterns are identified in many studies to gain a better understanding of mental disorders such as schizophrenia (SZ) either when compared with a healthy control (HC) group or in a longitudinal study (Weber et al., 2020; Rashid et al., 2014; Lefebvre et al., 2016).

In most previous dynamic studies that conduct a dFNC or dFC analysis, RSNs or ROIs are assumed to vary in their temporal coupling while staying constant spatially. DFNC is computed using association among the temporal variation patterns—time courses—of RSNs, which we refer to as tdFNC in this work. Spatial dynamics are increasingly being emphasized since they enrich the dynamic study of brain function (Iraji et al., 2019a, b; Iraji et al., 2020). Previous studies illustrate that taking both temporal and spatial variability into consideration yields more discriminative RSNs across subject groups (Jie et al., 2018; Kottaram et al., 2018). Studies that compute dFNC using spatial maps (sdFNC) of brain networks have emphasized the importance of spatial variability in a dynamic study. The analysis of sdFNC detects significant differences between the patients with a mental disorder such as between those with SZ and the HCs (Ma et al., 2014; Bhinge et al., 2019, 2020a). Therefore, it is desirable to accurately capture the spatial variability of RSNs in order to quantify and make use of the spatial variability as well as for studying the interaction between the temporal and spatial variability in dynamic studies.

Identifying discrete transient states of dFNC is a common strategy when studying the dynamic evolution of the brain function (Ma et al., 2014; Zhang et al., 2018). In each transient state, the dFNCs demonstrate unique characteristics compared with the others, indicating that unique connectivity patterns exist in these dFNCs. The determination of the number of states is an essential step, and is usually selected by using the lowest error/cost associated with the clustering methods that are used to identify the states. We propose to determine the number of states in a more interpretable way through a goal-driven scheme. In the study of brain function of patients with mental disorders, a key point is to find biomedical patterns that are unique for the patients when compared with a HC group. The use of a goal-driven scheme can thus help identify a scenario where a specific number of states with different discriminative features across groups are identified.

Graph-theoretical (GT) analysis has been widely used in the study of dFNC as they provide a simple and useful quantification of brain dynamics (Lee et al., 2017; Zhi et al., 2018). There are a variety of GT metrics defined to characterize FNC (Bullmore and Sporns, 2009; Telesford et al., 2020) and metrics that demonstrate significant group differences are of special interest. In this work, we investigate the effectiveness of GT analysis in identifying discriminative dynamic biomedical patterns that enable a unique characterization of dFNC states. We also demonstrate that a comprehensive study of the GT metrics in a goal-driven manner is a useful and effective approach for determining the number of states.

To ensure a successful GT analysis that yields discriminative GT metrics between groups, it is important to extract RSNs that preserve as much individual subject variability as possible. Independent vector analysis (IVA) is a data-driven technique that extends independent component analysis (ICA) to multiple datasets (Kim et al., 2006; Adalı et al., 2014). IVA has been shown to effectively capture the variability across the datasets compared with group ICA (Dea et al., 2011; Ma et al., 2013; Laney et al., 2014; Michael et al., 2014) and hence has been attractive for studying brain dynamics, especially when capturing both spatial and temporal variability (Ma et al., 2014; Bhinge et al., 2019, 2020a). However, IVA suffers from the dimensionality issue as the number of datasets and components increase beyond a certain range with a fixed number of samples in each observation (Bhinge et al., 2019; Long et al., 2020). A recent method, adaptively constrained IVA (acIVA), makes use of reference signals such as the spatial maps of RSNs to guide the decomposition. AcIVA inherits the property of IVA in capturing subject variabilities of RSNs in both temporal and spatial domains through an effective adaptively constraint parameter-tuning process. The use of reference signals guarantees a reliable decomposition and reduces the effect of high dimension issue to a certain extent Bhinge et al. (2020b). Moreover, acIVA enables the dynamic study of a set of target components such as those that are common across SZs and HCs, leading to a fair comparison of brain dynamics between the two groups.

Therefore, in this work, we propose the use of acIVA to effectively capture both the temporal and spatial variabilities of functional networks to enable a study of brain dynamics using resting-state fMRI data collected from SZs and HCs. We compute tdFNC and sdFNC by measuring correlation across the time courses and higher-order dependence across the spatial maps of the extracted RSNs separately and identify transient states by clustering tdFNC or sdFNC matrices. For each dFNC, different GT metrics, efficiency, characteristic path length, clustering coefficient, centrality, and small-worldness are calculated. Each state is characterized by summarizing the graph-level global GT metrics that show significant group differences. The results show that more GT metrics that are discriminative between groups are obtained when using sdFNC compared with using tdFNC, indicating that the spatial variability is highly informative for dynamic study. A comprehensive study of global GT metrics yields a scenario where all six identified sdFNC states are uniquely characterized. A following analysis of nodal metrics in this scenario demonstrate that the centrality is a key GT metric in this application. Four brain network components yield significantly different levels of involvement in SZ and HC groups regarding GT analysis results. The high involvement of a component that relates to multiple distributed brain regions—superior parietal, visual, and cerebellum—in SZs compared with HCs, points to dysconnectivity in the patients. Another component that relates to the supplementary motor area also yields higher involvement in SZs. We find that the HCs potentially possess a more efficient cognitive control system due to the high involvement of a frontoparietal component and a frontal component.

The rest of the paper is organized as follows. Section 2 introduces the details of acIVA algorithm and GT analysis. Section 3 gives the implementation details including data acquisition, preprocessing and formation, and reference signals extraction. Section 4 shows the results of dynamic study of resting-state fMRI data using acIVA and GT analysis. Section 5 summarizes the work and points out future directions.

2. Methods

2.1. Adaptively constrained IVA

ICA is a data-driven blind source separation technique that is designed for a single dataset with the assumption that the observed data is a linear mixture of latent (statistically) independent sources (Adalı et al., 2014; Hyvärinen et al., 2001). It has proven powerful in recovering the independent brain networks from fMRI data (Adalı et al., 2014; Calhoun et al., 2001; Li et al., 2009). However, the observed fMRI data typically consists of multiple datasets that are collected from multiple subjects. It is important to enable an analysis of multiset data to leverage its rich information, especially across multiple datasets. IVA extends ICA to the joint analysis of multiple datasets by additionally taking into account the dependence across datasets and has shown powerful in preserving subject variability (Ma et al., 2014; Bhinge et al., 2019, 2020a; Laney et al., 2014). Therefore, it is a desirable choice for the analysis of multi-subject fMRI data.

Given K datasets each containing V samples, IVA assumes that each dataset is a linear mixture of N independent sources,

$$\mathbf{x}^{[k]}(v) = \mathbf{A}^{[k]}\mathbf{s}^{[k]}(v),\ 1 \le k \le K,\ 1 \le v \le V, \tag{1}$$

where $\mathbf{X}^{[k]} = [\mathbf{x}^{[k]}(1),\ \mathbf{x}^{[k]}(2), \cdots,\ \mathbf{x}^{[k]}(V)] \in \mathbb{R}^{N\times V}$ denotes the observed dataset, $\mathbf{S}^{[k]} = \left[\mathbf{s}^{[k]}(1),\ \mathbf{s}^{[k]}(2), \cdots,\ \mathbf{s}^{[k]}(V)\right] \in \mathbb{R}^{N\times V}$ denotes the set of independent sources, and $\mathbf{A}^{[k]} \in \mathbb{R}^{N\times N}$ denotes the invertible mixing matrix. In addition to the assumption of independence among sources

within a dataset, IVA makes effective use of dependence across multiple datasets by defining a source component vector (SCV) as $\mathbf{s}_n(v) = \left[s_n^{[1]}(v), s_n^{[2]}(v), \cdots, s_n^{[K]}(v)\right]^{\mathrm{T}} \in \mathbb{R}^{K\times 1}$, $1 \le n \le N$, by collecting corresponding components, where $\mathbf{s}_n^{[k]} \in \mathbb{R}^{V\times 1}$ is the n th source from the k th dataset. IVA finds K demixing matrices by minimizing the mutual information among the SCVs, which results in the following cost function

$$\begin{aligned} \mathscr{J}(\mathscr{W}) &= \sum_{n=1}^{N} \mathscr{H}(\mathbf{y}_n) - \sum_{k=1}^{K} \log\left|\det \mathbf{W}^{[k]}\right| \\ &= \sum_{n=1}^{N} \mathscr{H}(\mathbf{y}_n) - \sum_{k=1}^{K}\sum_{n=1}^{N} \log\left|\left(\mathbf{h}_n^{[k]}\right)^{\mathrm{T}} \mathbf{w}_n^{[k]}\right| \end{aligned} \tag{2}$$

such that the estimated sources of each dataset are obtained as $\mathbf{y}^{[k]}(v) = \mathbf{W}^{[k]}\mathbf{x}^{[k]}(v)$ for $k = 1,\ldots,K$, where $\mathscr{W} = \{\mathbf{W}^{[1]}, \mathbf{W}^{[2]}, \cdots, \mathbf{W}^{[K]}\}$ denotes the demixing matrices, $\mathbf{y}_n$ denotes the estimated SCV, $\mathscr{H}(\cdot)$ denotes the (differential) entropy, and $\mathbf{h}_n^{[k]}$ is a unit vector that is perpendicular to all rows of $\mathbf{W}^{[K]}$ except $\mathbf{w}_n^{[k]}$ due to the decoupling process (Li and Zhang, 2007; Bhinge et al., 2017). Note the term that is associated with the observed data $\mathbf{X}$ is a constant with respect to $\mathbf{W}$, and hence it can be ignored.

The acIVA algorithm guides the decomposition with prior information such as properly selected reference signals for the source components. The IVA decomposition is hence achieved by minimizing the cost function in (2) subject to an inequality constraint $g(\mathbf{y}_n^{[k]}, \mathbf{d}_n) = \rho_n - \left|\left(\mathbf{y}_n^{[k]}\right)^{\mathrm{T}}\mathbf{d}_n\right| \le 0$, where $0 \le \rho_n \le 1$ is the constraint parameter that provides the lower bound for the similarity between the estimate $\mathbf{y}_n^{[k]}$ and the reference signal $\mathbf{d}_n$ that is measured using Pearson correlation. The cost function of acIVA is defined by incorporating the tinequality constraint in the IVA cost function, yielding

$$\begin{aligned} \mathscr{J}^{c}(\mathscr{W}) = \mathscr{J}(\mathscr{W}) - \sum_{m=1}^{M}\frac{1}{2\gamma_m}\sum_{k=1}^{K}\Big\{\left[\max\left\{0, \mu_m^{[k]} + \gamma_m g\left(\mathbf{y}_m^{[k]}, \mathbf{d}_m\right)\right\}\right]^2 \\ - \left(\mu_m^{[k]}\right)^2\Big\}, \end{aligned} \tag{3}$$

where $\mathscr{J}(\mathscr{W})$ is the IVA cost function as defined in (2), M $(0 \le M \le N)$ is the number of source estimates to be constrained, $\mu_m^{[k]}$ is the regularization parameter, and $\gamma_m > 0$ is the penalty parameter (Bhinge et al., 2019). Through an adaptive parameter-tuning process, acIVA yields different values of the lower bound $\hat{\rho}$ for the similarity, which allows the estimate to vary across datasets. Consequently, acIVA is able to effectively capture the variability across datasets. The use of reference signals effectively reduces the effect of high dimensionality in IVA, enabling a more robust estimation. Additionally, it eliminates the alignment problem across multiple decompositions.

2.2. GT analysis

We compute dFNC for each subject by measuring the associations across the components of interest—the constrained estimates in acIVA—and conduct a GT analysis on dFNC matrices. Each dFNC matrix is a graph, $\mathbf{G}$, with the components used as nodes and the association—either correlation or mutual information—among them as edges. Beginning with $\mathbf{G}$, we arrange its edges from the smallest to the largest and find an edge threshold, e_t, in order to retain P percent of the edges that satisfy $e \le e_t$, generating a new graph $\mathbf{G}'$. We define the percentage of edges that remain after thresholding as the link density, which increases as the threshold decreases. All GT metrics are computed for the weighted graphs. In order to avoid very sparse graphs with small link densities and those with too high link densities, we limit the link density to range from 20 % to 70 %.

GT metrics highlight different topological characteristics of graphs, see *e.g.*, (Bullmore and Sporns, 2009; Boccaletti et al., 2006; Bullmore and Bassett, 2011). The characteristic path length, global efficiency and centrality are measures that can quantify the ability of a node to facilitate functional integration in graphs (Rubinov and Sporns, 2010). These nodal GT metrics are globally computed as all the nodes are taken into consideration in their calculation, and provide measures of how information is transferred in the functional network. Local efficiency and clustering coefficient are two local nodal GT metrics that are computed by taking only the neighbors of a node into consideration. The local efficiency measures the efficiency of information transfer within the neighborhood of each node. The clustering coefficient captures the segregation of networks by measuring the transfer of information in the immediate neighborhood of each node. The corresponding graph-level global GT metric is computed by averaging the values of each nodal GT metric across all the nodes in a graph. Another graph-level global GT metric, small-worldness of the network, is calculated to measure the degree of small-world organization in the overall functional network. The formulas of these metrics are described in detail in (Rubinov and Sporns, 2010; Bonacich, 1987, 2007).

3. Implementation

The implementations are performed using Matlab code provided in the Group ICA of fMRI Toolbox (GIFT) (http://trendscenter.org/soft

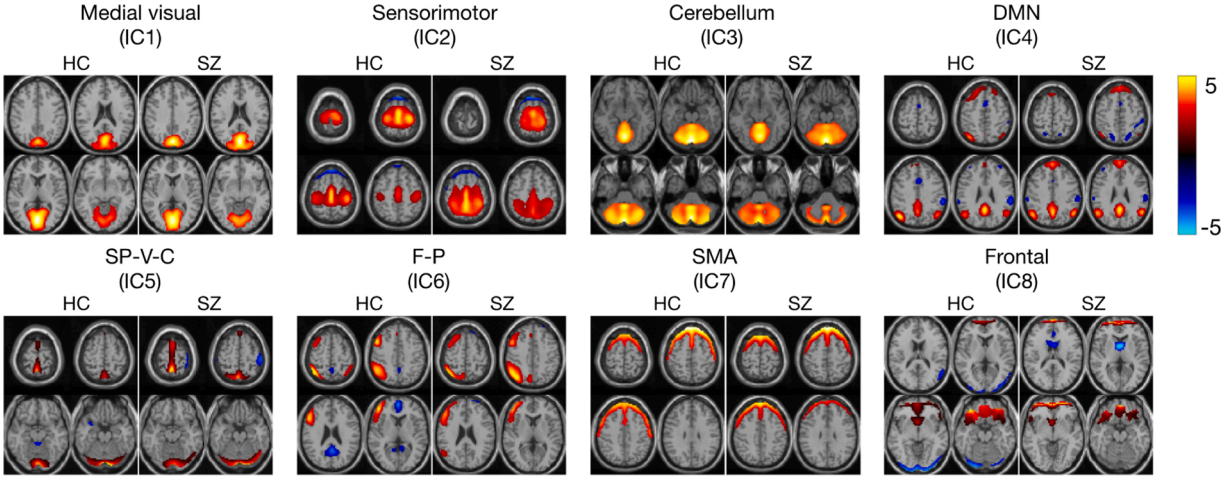

Fig. 1. Spatial maps of the eight common components of HC and SZ groups. SP-V-C: super parietal-visual-cerebellum, F-P: frontoparietal, SMA: supplementary motor area.

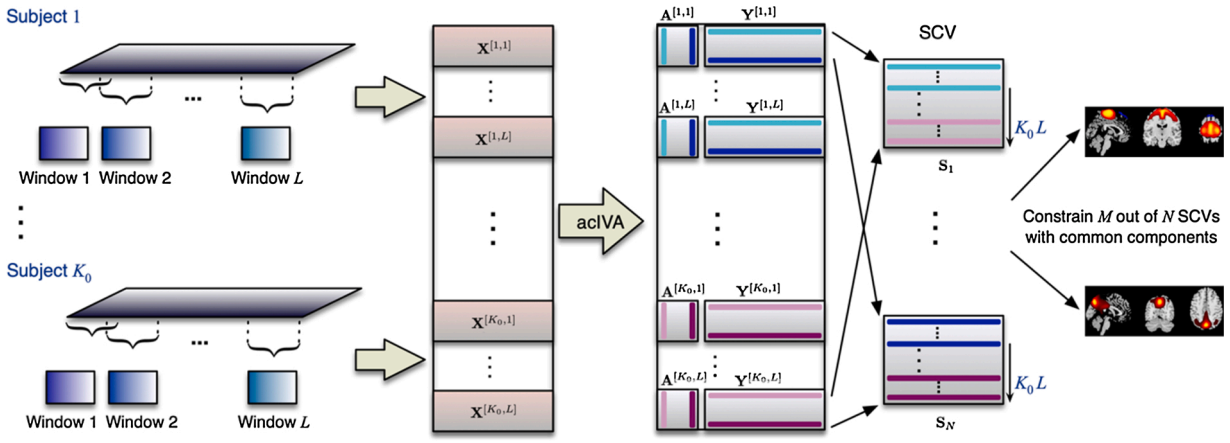

Fig. 2. Dynamic study using acIVA with windowing strategy.

ware/gift) that also has a number of IVA algorithms included, and the Brain Connectivity Toolbox (https://sites.google.com/site/bctnet/).

3.1. Data acquisition and preprocessing

We use a resting state fMRI data from the Center of Biomedical Research Excellence (COBRE) that is available on the collaborative informatics and neuroimaging suite data exchange repository (https://coins.trendscenter.org/) (Scott et al., 2011; Çetin et al., 2014). The data includes 88 SZs (average age: 37 ± 14) and 91 HCs (average age: 38 ± 12). All images were collected on a single 3-Tesla Siemens Trio scanner with a 12-channel radio frequency coil using the following parameters: TE =29 ms, TR = 2 s, flip angle = 75°, slice thickness = 3.5 mm, slice gap = 1.05 mm, voxel size $3.75 \times 3.75 \times 4.55$ mm^3. Participants were instructed to keep their eyes open during the scan and stare passively at a central fixation cross. Each resting state scan consists of 150 volumes. To eliminate the T1-related signal fluctuations (T1 effect) (Shin et al., 2013), the first 6 volumes are removed in this study, thus 144 volumes remain for each subject. The fMRI data are realigned with INRIalign algorithm (Freire et al., 2002) for head motion correction, followed by slice-timing correction to account for timing difference by using the middle slice as the reference frame. Then the fMRI data are spatially normalized to the standard Montreal Neurologic Institute space and resampled to $3 \times 3 \times 3$ mm^3, resulting in $53 \times 63 \times 46$ voxels. Afterwards, the fMRI data are smoothed using a Gaussian kernel with a full-width at half-maximum of 5 mm.

3.2. Reference signal extraction

We use exemplar RSN components as the reference signals within the acIVA framework. Potential choices include the pre-defined RSN templates (Allen et al. (2011)) and the group-level RSN components that are extracted from the same dataset using group decomposition algorithms such as group ICA (Bhinge et al., 2020a). The data we use in this work is the resting-state fMRI collected from subjects with SZ and a HC group. In order to conduct a fair comparison between the SZ and HC groups, we extract the common RSN components that are shared across the two groups as the reference signals. We make use of a recent common subspace extraction framework, IVA for common subspace analysis (IVA-CS) (Long et al. (2020)), to estimate the independent components (IC), yielding $M = 8$ common RSNs as shown in Fig. 1. The eight common RSNs include the medial visual (IC1), the sensorimotor (IC2), the cerebellum (IC3), the DMN (IC4), a component that includes multiple distributed brain regions—the super parietal, visual, and cerebellum cortex—(SP-V-C, IC5), the frontoparietal (F-P, IC6), the supplementary motor area (SMA, IC7), and the frontal (IC8) components. The spatial maps of the eight RSNs are used as reference signals in acIVA decompositions. All the spatial maps are normalized to have zero mean and unit variance.

3.3. Dynamic study using acIVA

FMRI data is obtained by scanning the brain within a certain duration of multiple minutes. The sliding window approach is widely used to facilitate a dynamic study of fMRI data by dividing the scanning period into overlapping windows (Hutchison et al., 2013b; Ma et al., 2014; Savva et al., 2020). The data in each window forms an individual new dataset. We use a sliding window of length $T_w = 24$ (48 s) with a 66.67 % overlap as shown in Fig. 2, yielding $L = 16$ datasets for each of the 179 subjects. The dynamics can be described using FNC information across the 16 windows. The total number of datasets to be analyzed for the extraction of functional networks is $L \times 179 = 2864$. We propose the use of acIVA to capture the dynamics by effectively analyzing a relatively large number of datasets. Since acIVA mitigates the dimensionality issue and eliminates the alignment problem across multiple decompositions, we divide the 2864 datasets into 45 subsets of 64 datasets ($K_0 = 4$ subjects), a value that is higher than the optimal value of the number of datasets that allows a reliable regular IVA decomposition (Long et al., 2020), and perform acIVA on each subset. Note that the last subset of HC group only has three subjects hence 48 datasets.

The model order—the number of source components—in each acIVA decomposition is set as 20 and the dimension of each dataset is reduced from 24 to 20 using principal component analysis. We select 20, a value that is slightly lower than the original dimension of each dataset as the model order in order to reduce the influence of noise while retaining a significant level of signal variability. Eight of the estimates are constrained by the spatial maps of the common exemplar RSNs. We set the penalty parameter $\gamma_m = 3$ for all constrained components and initialize the regularization parameter $\mu_m^{[k]} = 0$. During the decomposition, we update the regularization parameter using $\mu_m^{[k]} = \max\left\{0, \mu_m^{[k]} + \gamma_m g\left(\mathbf{y}_m^{[k]}, \mathbf{d}_m\right)\right\}$ and tune the value of ρ_m from a candidate set $\mathscr{P}$ for each of the constrained components (Bhinge et al., 2019). In our implementation, we chose the set as $\mathscr{P} = \{0.1, 0.2, 0.3, 0.4, 0.5, 0.6, 0.7, 0.8, 0.9\}$ and one can choose to be even more conservative and can include correlation values in smaller steps, *e.g.*, steps of 0.05. The tdFNC is computed as the correlation among the time courses and the sdFNC is computed as the normalized mutual information among the spatial maps. For each type of dFNC, a k-means clustering is performed to identify the transient states with different values as the number of states, $N_s = 3, 4, 5, 6, 7, 8, 9, 10, 11, 12$, to enable an extensive investigation of the influence of N_s.

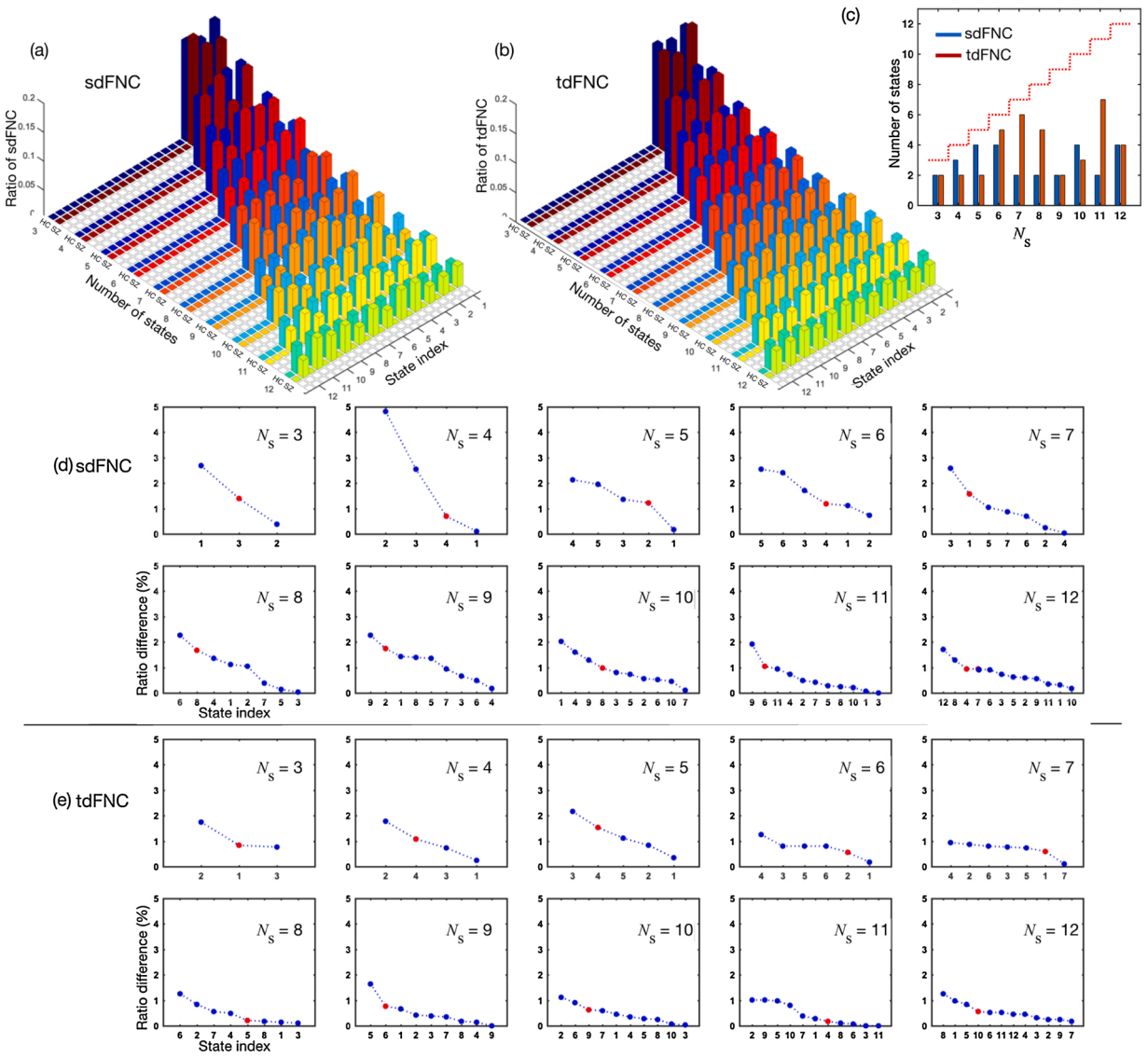

Fig. 3. Ratio of the number of dFNC matrices in each state for SZ and HC groups as the value of N_s changes when using sdFNC (a) and tdFNC (b). The number of states with different ratios between the two groups is summarized in (c). The results of the knee point detection for states with different ratios between the two groups are shown in (d) for sdFNC and (e) for tdFNC.

3.4. A goal-driven scheme for the determination of N_s

By applying acIVA to the dynamic study of the resting-state COBRE fMRI data collected from SZ subjects and HCs, our goal is to identify dynamic biomedical patterns with significant group difference. Analyzing these discriminative dynamic patterns helps us understand functional differences in the brain between groups, enabling a better interpretation of SZ. We perform a GT analysis on the dFNC matrices and calculate different GT metrics by changing the link density in each dFNC as described in Section 2.2. A two-sample t-test is performed on each GT metric between the SZs and HCs in each state in order to determine whether the metric yields values that are significantly different between the two groups. The detected significance is reported with the false discovery rate (FDR) control. Along with the goal of identifying discriminative biomedical features, we propose the use of a goal-driven scheme to investigate the influence of N_s. This comprehensive study of GT metrics identifies metrics that are discriminative between groups and notifies how the discriminative metrics change across states. It would be desirable if in the scenario of the optimal N_s, all the identified states yield discriminative GT metrics that are different in terms of the number and types of metrics.

4. Results

4.1. Transient states

We give an overview of the properties of identified transient states in Fig. 3 and show that all states contain dFNCs that are from both the HC and SZ groups. In each state, we calculate the ratio of sdFNC/tdFNC matrices for the SZ and HC groups separately and summarize them in Fig. 3(a) and (b). We compare the ratio of sdFNC/tdFNC between the two groups and show the difference in Fig. 3(d) and (e). We then find the knee point for the ratio differences by using an elbow criterion that is calculated as the ratio of within-cluster distance to between-cluster distance (Zhang et al., 2018; Vergara et al., 2020). The points before the knee point have large ratio differences, indicating that the number of sdFNC/tdFNC matrices are obviously different between SZ and HC groups in corresponding states. In Fig. 3(c), we show the number of states with a large ratio difference. When using tdFNC, the number of states with a large ratio difference is the largest (7) when $N_s = 11$. While when using sdFNC, the number of states with a large ratio difference is bounded between 2 and 4. The results indicate that the identified states using sdFNC are more balanced between SZ and HC groups regarding

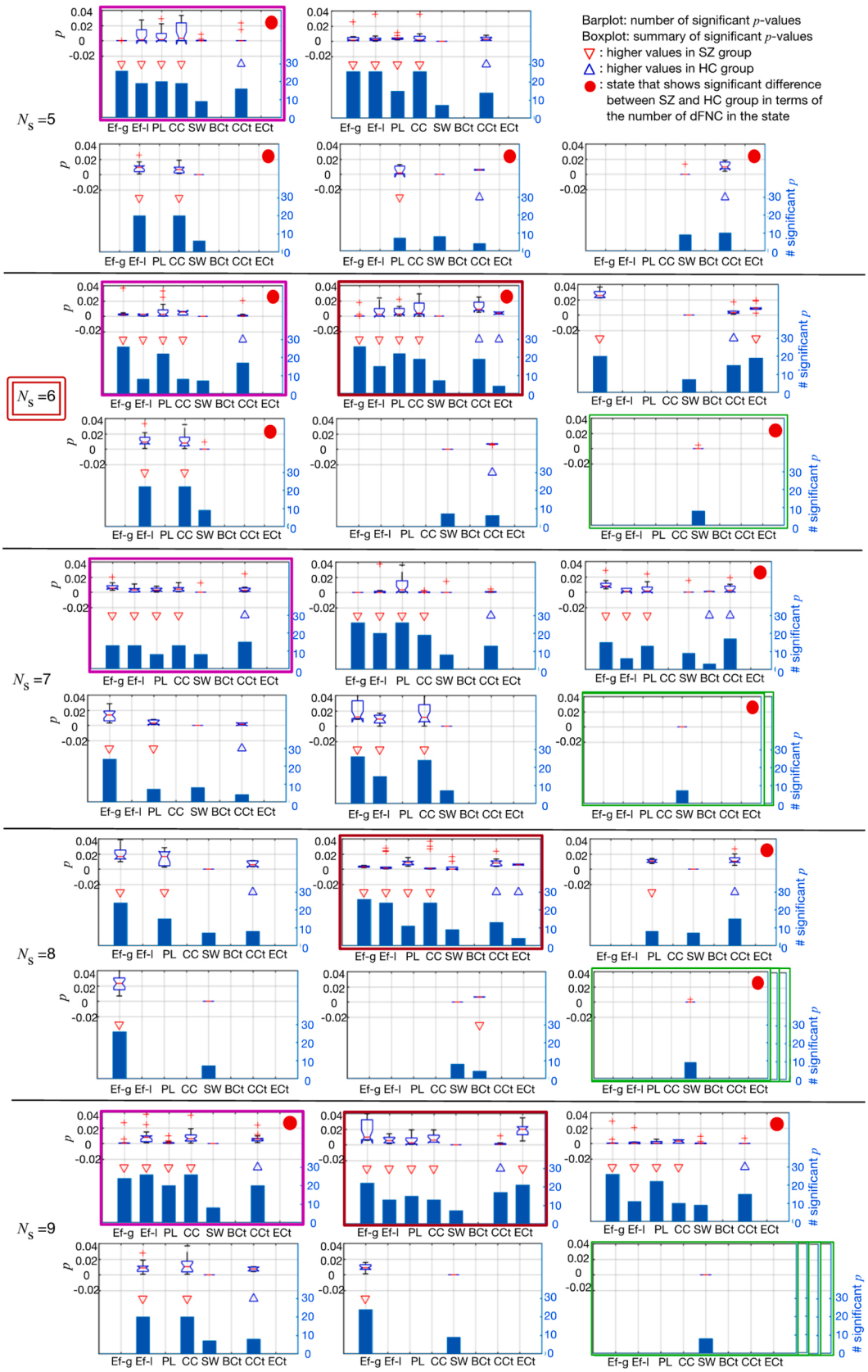

Fig. 4. Summary of the statistical test results of global GT metrics in five cases for sdFNC. Overlapping plots for $N_s = 7, 8, 9$ means more than one states have the same characteristics. In each plot, the boxplot on the top summarizes the p -values with FDR control, the barplot gives the number of graphs with different link density that have a significant p -value, and the triangular over a bar means the GT metric has higher value in SZs (red) or HCs (blue). The red dot in the upper right corner indicates the number of SZ and HC subjects are different in a state. Ef-g: global efficiency, Ef-l: local efficiency, PL: path length, CC: clustering coefficient, SW: small-worldness, BCt: betweenness centrality, CCt: closeness centrality, ECt: eigenvector centrality.

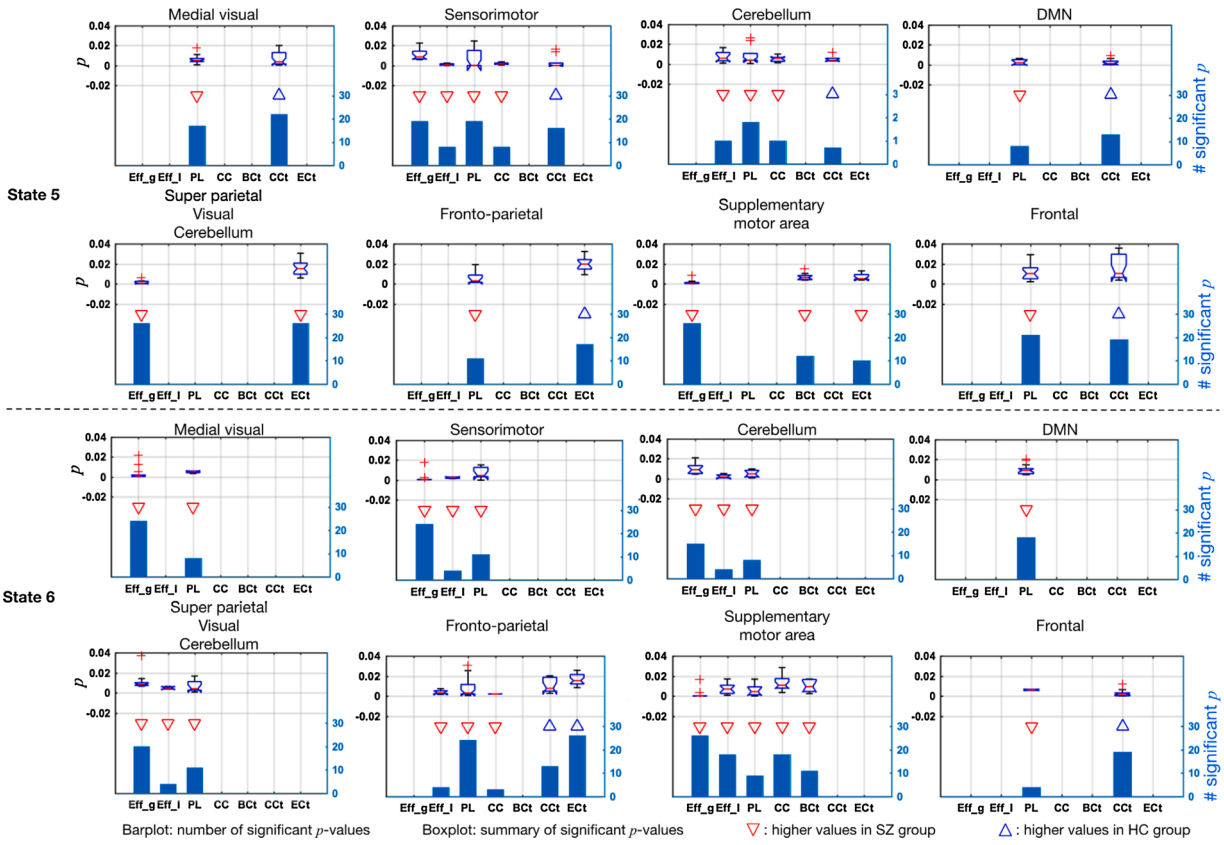

Fig. 5. Summary of the statistical test results of nodal GT metrics for states 5 and 6 when $N_s = 6$. In each plot, the boxplot on the top summarizes the p -values with FDR control, the barplot gives the number of graphs with different link density that have a significant p -value, and the triangular over a bar means the test results show the GT metric has higher value in SZs (red) or HCs (blue). Ef-g: global efficiency, Ef-l: local efficiency, PL: path length, CC: clustering coefficient, BCt: betweenness centrality, CCt: closeness centrality, ECt: eigenvector centrality.

the number of dFNC matrices.

4.2. GT analysis

In this work, the statistical tests illustrate that the number of discriminative GT metrics that demonstrate significant differences between the HC and SZ groups is much less for tdFNC compared with sdFNC. The type of discriminative GT metrics is humdrum and the clustering coefficient and small-worldness always demonstrate significant differences for tdFNC. Therefore, whatever the value of N_s is, most of the states have the same characteristics in terms of discriminative global GT metrics as we demonstrate in Figs. S1 and S2 in the supplementary material. In contrast, sdFNC yields more discriminative GT metrics and the number and type of these discriminative metrics vary across states as shown in Fig. 4, making it possible to uniquely characterize the states by using these discriminative metrics. Moreover, this suggests that the highly informative spatial variability provides more chances to identify unique biomedical patterns of the subjects with SZ in this study. We also study the relationship between the two types of measure for sdFNC—the correlation and the mutual information values—and find that they are coherent. We believe that both are good choices, but choose to use mutual information that captures the higher-order statistical information for sdFNC to make a better use of the high number of samples in the spatial domain. Next, we introduce the quantitative study of sdFNC using GT analysis and determine the value of N_s for sdFNC.

We summarize the two-sample t -test results of the global GT metrics in Fig. 4 for sdFNC. There are ten cases with different values of $N_s \in \{3, 4, 5, 6, 7, 8, 9, 10, 11, 12\}$ and we show five cases, $N_s = 5, 6, 7, 8, 9$, as examples. In each plot, the boxplot on the top summarizes the significant p -values with FDR control, the barplot gives the number of graphs with different levels of link density that yield discriminative GT metrics, and the triangular over a bar means the GT metric has higher values in SZs (red) or HCs (blue). If there is no triangular over a bar, it means among the graphs some have higher metric values in the SZ group while the others have higher metric values in the HC group. The red dot in the upper right corner indicates the number of sdFNC matrices are not balanced in SZ and HC groups in a state. There are three states, as labeled in magenta, red, and green rectangular separately, that are robustly estimated. When $N_s \leq 5$, there are missing states compared with the cases where $N_s \geq 6$. The cases with $N_s \geq 7$ yield multiple states that are not discriminative through the characterization using a summary of global GT metrics, as we show in Fig. 4 using the overlapping figures with a green box for cases of $N_s = 7, 8, 9$. Therefore, $N_s = 6$ is the optimal case where all six states are unique. The results illustrate that the comprehensive study of the global GT metrics effectively determines of the optimal number of states N_s. We also use the elbow approach to estimate the optimal value of N_s. The mean value and standard deviation of 100 runs are 6.02 ± 0.94, coinciding with the value suggested by studying the GT metrics. However, the study of GT metrics determines the optimal value of N_s in a more interpretable way by looking into the discriminative GT features that help us compare between groups.

We also investigate the nodal GT metrics in the case of $N_s = 6$ in order to find interesting individual RSNs. We show two states, states 5 and 6, in Fig. 5 where all eight components have at least one discriminative GT metric. In state 5, only the multi-region component (IC5) and the supplementary motor component (IC7) that consists of superior and middle frontal cortex yield higher values of centrality in SZ, while the other six components yield higher values of centrality in HC. This high

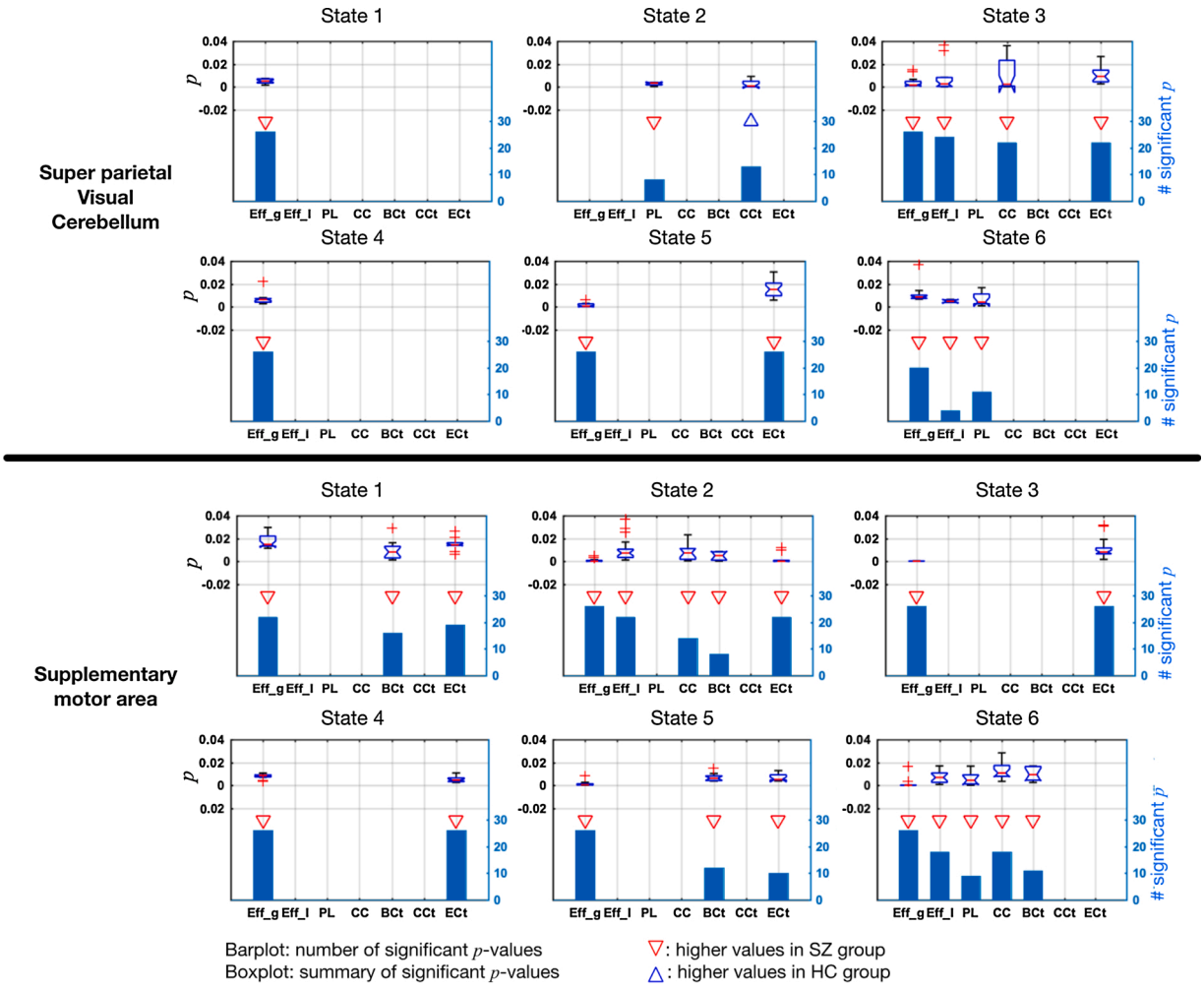

Fig. 6. Summary of the statistical test results of nodal GT metrics for the complex component (IC5) and the supplementary motor area component (IC7) when $N_s = 6$. In each plot, the boxplot on the top summarizes the p -values with FDR control, the barplot gives the number of graphs with different link density that have a significant p -value, and the triangular over a bar means the test results show the GT metric has higher value in SZs (red) or HCs (blue). Ef-g: global efficiency, Ef-l: local efficiency, PL: path length, CC: clustering coefficient, BCt: betweenness centrality, CCt: closeness centrality, ECt: eigenvector centrality.

centrality of IC5 infers that the SZ subjects tend to have more brain regions involved for a certain intrinsic brain function, illustrating the dysconnectivity in the brain of SZ. In state 6, the frontoparietal component IC6 and frontal component IC8 yield higher values of centrality in HC compared with SZ, potentially suggesting a more efficient cognitive control system in the brain of HCs.

The two components IC5 and IC7 even yield discriminative GT metrics in all six states, as shown in Fig. 6. Except for the closeness centrality in state 2 for IC5, the values of all the other GT metrics are higher in SZ group than in HC group, indicating the increased involvement of the two components in the brain function of SZs. The increased involvement of the multi-region component IC5 once more suggests dysconnectivity in SZ brain function. The other component IC7 that consists of superior and middle frontal cortex has been reported in many studies to have different levels of activation in SZ compared with HC. In Fig. 7, we show the GT metrics for the other two interesting components, IC6, the frontoparietal component, and IC8, the frontal component, that yield discriminative GT metrics in five and four states separately. All the values of centrality are higher in HCs in these states. The high involvement of IC6 and IC8 again supports the conclusion that HCs and SZs demonstrate differences in their cognitive control system.

From the analysis of nodal GT metrics, we note that the most interesting GT metric is the centrality. An analysis of centrality yields differences among individual components in terms of their role on the brain function. Four interesting RSN components that yield interpretable GT analysis results include the multi-region component IC5, the supplementary motor component IC7, the frontoparietal component IC6 and the frontal component IC8. A study of these four components helps get a better understanding of the differences between the brain function of SZs and HCs, *i.e.*, the dysconnectivity in the brain of SZs and an efficient cognitive control system for HCs.

5. Conclusion and future directions

In this work, we propose the use of acIVA to capture both temporal and spatial variation of brain functional networks to enable a thorough study of brain dynamics. We emphasize the importance of taking spatial variability into consideration in the dynamic study of fMRI data by conducting a GT analysis on tdFNC and sdFNC. The results show that the rich dynamic information in the spatial domain yields more features that are potentially unique biomedical patterns of subjects with SZ. In order to identify transient states to learn the dynamic evolution of brain function, we propose the use of a goal-driven scheme—the systematic study of GT metrics in this work—to determine the optimal value for the number of states N_s. The results illustrate that the proposed scheme successfully finds a case where the value of N_s is optimal in a more interpretable way compared with using an arbitrary statistical method. In the case with the optimal $N_s = 6$, all six states are uniquely charac-

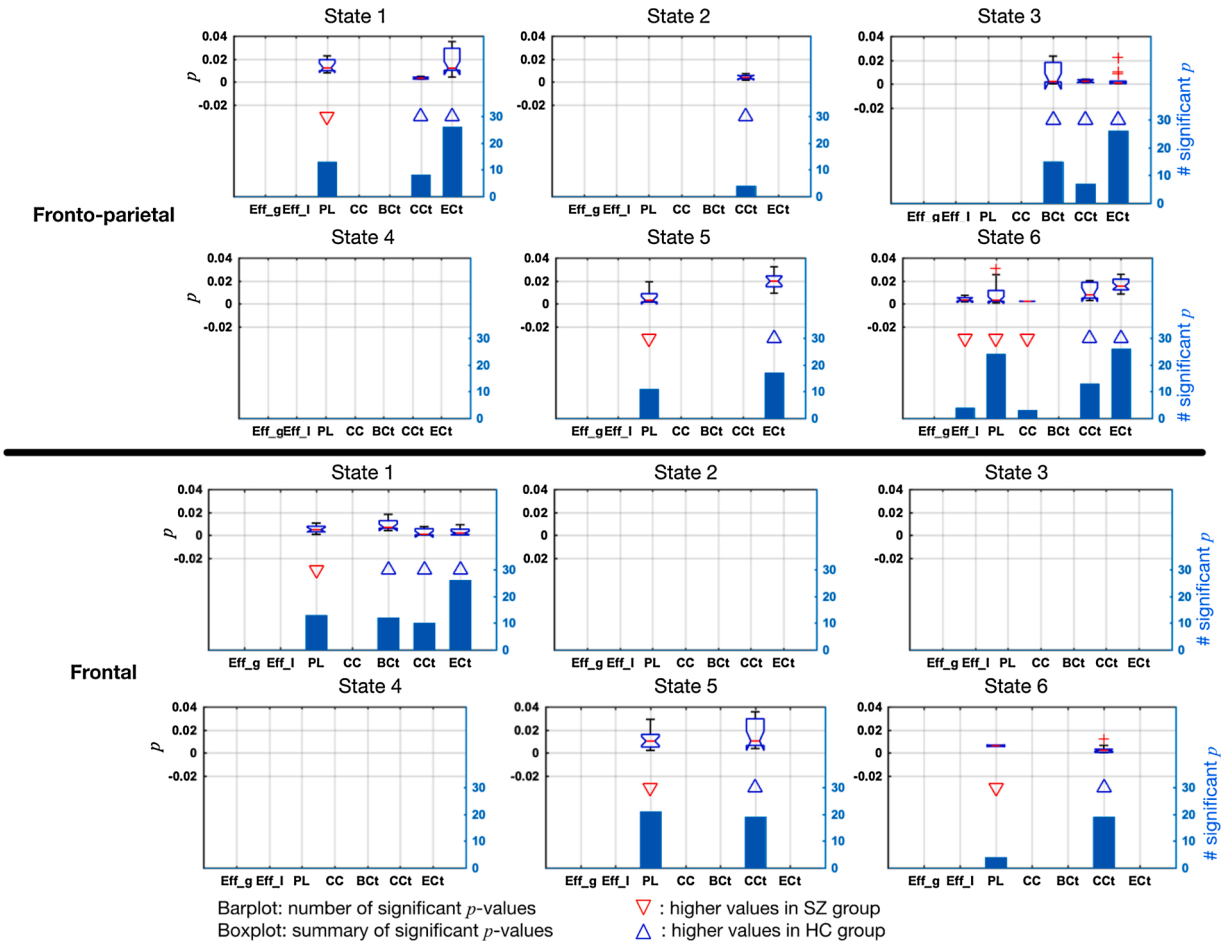

Fig. 7. Summary of the statistical test results of nodal GT metrics for the frontoparietal component (IC6) and the supplementary motor area component (IC7) when $N_s = 6$. In each plot, the boxplot on the top summarizes the p -values with FDR control, the barplot gives the number of graphs with different link density that have a significant p -value, and the triangular over a bar means the test results show the GT metric has higher value in SZs (red) or HCs (blue). Ef-g: global efficiency, Ef-l: local efficiency, PL: path length, CC: clustering coefficient, BCt: betweenness centrality, CCt: closeness centrality, ECt: eigenvector centrality.

terized by the global GT metrics. The study of nodal GT metrics in these states demonstrates that the centrality is the most interesting metric in this application. Four interesting components that yield interpretable GT analysis results include a multi-region component, a supplementary motor component, a frontoparietal component and a frontal component. The multi-region component demonstrates increased involvement in the brain function of SZs compared with HCs, illustrating dysconnectivity among the SZ brain networks. Frontoparietal and frontal components yield higher values of centrality in HCs, potentially suggesting a more efficient cognitive control system in the brain of HCs.

We demonstrate the importance of taking spatial variability into consideration and propose the use of a goal-driven scheme for the determination of the number of states in dFNC analysis by applying acIVA and GT analysis to the resting-state COBRE data. We focused the analysis on the eight common components. However, one can also investigate the contribution of components that are unique in either the HC group or the SZ group to dFNC analysis. We were not able to conduct a performance comparison with existing algorithms such as group ICA (Calhoun et al., 2001) and regular IVA due to the unique advantage of acIVA that it can focus the analysis on a set of target components. The requirements of low orders and low noise levels in the tensor decomposition models like canonical polyadic decomposition and block-term decomposition (Stegeman, 2020; Sorber et al., 2015; Chatzichristos et al., 2019) also limit the applicability of these other factorization methods for a dynamics study. Though it is not easy to make a comparison with the existing methods in real fMRI analysis, we have conducted a detailed simulation study that helps demonstrate the effectiveness of acIVA (Bhinge et al., 2019; Long et al., 2020; Bhinge et al., 2020b). We showed that acIVA is able to tune the closest lower bound for the association between the reference signals and the constrained components without introducing any artificial connection. We also illustrated that acIVA successfully preserved variabilities of datasets and reduced the effect of dimensionality issue. Nevertheless, it might be desirable to extend the work to other fMRI datasets and other neuroimaging modalities to gain more evidence. The GT analysis has shown powerful in FNC study but is also worthy to be investigated more for dynamic analysis, exploring more possibilities to make use of discriminative GT metrics.

Funding statement

Qunfang Long, Suchita Bhinge, Vince D. Calhoun, and Tulay Adali were supported by NSF grants CCF 1618551 and NCS 1631838, and NIH grant R01MH 118695. Vince D. Calhoun was also supported by NIH grant R01EB 020407.

CRediT authorship contribution statement

Qunfang Long: Formal analysis, Investigation, Methodology, Software, Validation, Visualization, Writing - original draft. **Suchita Bhinge:** Methodology, Investigation. **Vince D. Calhoun:** Data curation, Funding acquisition, Resources, Writing - review & editing. **Tülay**

Adali: Funding acquisition, Project administration, Resources, Supervision, Writing - review & editing.

Declaration of Competing Interest

The authors report no declarations of interest.

Acknowledgments

This work was supported by NSF grants CCF 1618551 and NCS 1631838, and NIH grants R01MH 118695 and R01EB 020407. The authors thank the research staff from the Mind Research Network COBRE study who collected, preprocessed and shared the data. The authors appreciate valuable feedback provided by the members of Machine Learning for Signal Processing Laboratory at the University of Maryland, Baltimore County.

Appendix A. Supplementary data

Supplementary material related to this article can be found, in the online version, at doi:https://doi.org/10.1016/j.jneumeth.2020.109039.

References

Adalı, T., Anderson, M., Fu, G.-S., 2014. Diversity in independent component and vector analyses: Identifiability, algorithms, and applications in medical imaging. IEEE Signal Process. Mag. 31 (3), 18–33. https://doi.org/10.1109/MSP.2014.2300511.

Allen, E.A., Erhardt, E.B., Damaraju, E., Gruner, W., Segall, J.M., Silva, R.F., Havlicek, M., Rachakonda, S., Fries, J., Kalyanam, R., et al., 2011. A baseline for the multivariate comparison of resting-state networks. Front. Syst. Neurosci. 5, 2.

Bhinge, S., Long, Q., Levin-Schwartz, Y., Boukouvalas, Z., Calhoun, V.D., Adalı, T., 2017. Non-orthogonal constrained independent vector analysis: application to data fusion, in: Acoustics, Speech and Signal Processing (ICASSP). 2017 IEEE International Conference on 2666–2670.

Bhinge, S., Mowakeaa, R., Calhoun, V.D., Adalı, T., 2019. Extraction of time-varying spatiotemporal networks using parameter-tuned constrained IVA. IEEE Trans. Med. Imaging 38 (7), 1715–1725.

Bhinge, S., Long, Q., Calhoun, V.D., Adali, T., 2020a. Spatial dynamic functional connectivity analysis identifies distinctive biomarkers in schizophrenia. Front. Neurosci. 13.

Bhinge, S., Long, Q., Vince, C.D., Adali, T., 2020b. Adaptive constrained independent vector analysis: an effective solution for analysis of large-scale medical imaging data. IEEE J. Sel. Top. Signal Process.

Boccaletti, S., Latora, V., Moreno, Y., Chavez, M., Hwang, D.-U., 2006. Complex networks: Structure and dynamics. Phys. Rep. 424 (4), 175–308.

Bonacich, P., 1987. Power and centrality: A family of measures. Am. J. Sociol. 92 (5), 1170–1182.

Bonacich, P., 2007. Some unique properties of eigenvector centrality. Soc. Networks 29 (4), 5.

Bullmore, E.T., Bassett, D.S., 2011. Brain graphs: Graphical models of the human brain connectome. Annu. Rev. Clin. Psychol. 7, 113–140.

Bullmore, E., Sporns, O., 2009. Complex brain networks: Graph theoretical analysis of structural and functional systems. Nat. Rev. Neurosci. 10 (3), 186–198.

Calhoun, V.D., Adalı, T., Pearlson, G.D., Pekar, J.J., 2001. A method for making group inferences from functional MRI data using independent component analysis. Hum. Brain Mapp. 14 (3), 140–151.

Calhoun, V.D., Miller, R., Pearlson, G., Adalı, T., 2014. The chronnectome: Time-varying connectivity networks as the next frontier in fMRI data discovery. Neuron 84 (2), 262–274.

Çetin, M.S., Christensen, F., Abbott, C.C., Stephen, J.M., Mayer, A.R., Cañive, J.M., Bustillo, J.R., Pearlson, G.D., Calhoun, V.D., 2014. Thalamus and posterior temporal lobe show greater inter-network connectivity at rest and across sensory paradigms in schizophrenia. NeuroImage 97, 117–126.

Chang, C., Glover, G.H., 2010. Time–frequency dynamics of resting-state brain connectivity measured with fMRI. NeuroImage 50 (1), 81–98.

Chatzichristos, C., Kofidis, E., Morante, M., Theodoridis, S., 2019. Blind fMRI source unmixing via higher-order tensor decompositions. J. Neurosci. Methods 315, 17–47.

Chen, B., 2019. Abnormal cortical region and subsystem complexity in dynamical functional connectivity of chronic schizophrenia: A new graph index for fMRI analysis. J. Neurosci. Methods 311, 28–37.

Dea, J.T., Anderson, M., Allen, E., Calhoun, V.D., Adalı, T., 2011. IVA for multi-subject fMRI analysis: a comparative study using a new simulation toolbox. In: 2011 IEEE International Workshop on Machine Learning for Signal Processing. IEEE, pp. 1–6.

Freire, L., Roche, A., Mangin, J.-F., 2002. What is the best similarity measure for motion correction in fMRI time series? IEEE Trans. Med. Imaging 21 (5), 470–484.

He, C., Chen, Y., Jian, T., Chen, H., Guo, X., Wang, J., Wu, L., Chen, H., Duan, X., 2018. Dynamic functional connectivity analysis reveals decreased variability of the default-mode network in developing autistic brain. Autism Res. 11 (11), 1479–1493.

Hutchison, R.M., Womelsdorf, T., Gati, J.S., Everling, S., Menon, R.S., 2013a. Resting-state networks show dynamic functional connectivity in awake humans and anesthetized macaques. Hum. Brain Mapp. 34 (9), 2154–2177.

Hutchison, R.M., Womelsdorf, T., Allen, E.A., Bandettini, P.A., Calhoun, V.D., Corbetta, M., Della Penna, S., Duyn, J.H., Glover, G.H., Gonzalez-Castillo, J., et al., 2013b. Dynamic functional connec- tivity: promise, issues, and interpretations. NeuroImage 80, 360–378.

Hyvärinen, A., Karhunen, J., Oja, E., 2001. Independent Component Analysis. John Wiley & Sons, Inc.

Iraji, A., Fu, Z., Damaraju, E., DeRamus, T.P., Lewis, N., Bustillo, J.R., Lenroot, R.K., Belger, A., Ford, J.M., McEwen, S., et al., 2019a. Spatial dynamics within and between brain functional domains: a hierarchical approach to study time-varying brain function. Hum. Brain Mapp. 40 (6), 1969–1986.

Iraji, A., Deramus, T.P., Lewis, N., Yaesoubi, M., Stephen, J.M., Erhardt, E., Belger, A., Ford, J.M., McEwen, S., Mathalon, D.H., et al., 2019b. The spatial chronnectome reveals a dynamic interplay between functional segregation and integration. Hum. Brain Mapp. 40 (10), 3058–3077.

Iraji, A., Miller, R., Adali, T., Calhoun, V.D., 2020. Space: A missing piece of the dynamic puzzle. Trends Cogn. Sci. 24 (2), 135–149.

Jafri, M.J., Pearlson, G.D., Stevens, M., Calhoun, V.D., 2008. A method for functional network connectivity among spatially independent resting-state components in schizophrenia. NeuroImage 39 (4), 1666–1681.

Jie, B., Liu, M., Shen, D., 2018. Integration of temporal and spatial properties of dynamic connectivity networks for automatic diagnosis of brain disease. Med. Image Anal. 47, 81–94.

Kim, T., Eltoft, T., Lee, T.-W., 2006. Independent vector analysis: an extension of ica to multivariate com- ponents. International Conference on Independent Component Analysis and Signal Separation 165–172.

Kottaram, A., Johnston, L., Ganella, E., Pantelis, C., Kotagiri, R., Zalesky, A., 2018. Spatio-temporal dynamics of resting-state brain networks improve single-subject prediction of schizophrenia diagnosis. Hum. Brain Mapp. 39 (9), 3663–3681.

Kucyi, A., Davis, K.D., 2014. Dynamic functional connectivity of the default mode network tracks day-dreaming. NeuroImage 100, 471–480.

Laney, J., Westlake, K., Ma, S., Woytowicz, E., Adalı, T., 2014. Capturing subject variability in data driven fMRI analysis: a graph theoretical comparison. 48th Annual Conference on Information Sciences and Systems (CISS) 1–6. https://doi.org/10.1109/CISS.2014.6814109.

Lee, N., Kim, J.-M., 2019. Dynamic functional connectivity analysis of functional MRI based on copula time-varying correlation. J. Neurosci. Methods 323, 32–47.

Lee, W.H., Bullmore, E., Frangou, S., 2017. Quantitative evaluation of simulated functional brain networks in graph theoretical analysis. NeuroImage 146, 724–733.

Lefebvre, S., Demeulemeester, M., Leroy, A., Delmaire, C., Lopes, R., Pins, D., Thomas, P., Jardri, R., 2016. Network dynamics during the different stages of hallucinations in schizophrenia. Hum. Brain Mapping 37 (7), 2571–2586.

Li, K., Guo, L., Nie, J., Li, G., Liu, T., 2009. Review of methods for functional brain connectivity detection using fMRI. Comput. Med. Imaging Graph. 33 (2), 131–139.

Li, X.-L., Zhang, X.-D., 2007. Nonorthogonal joint diagonalization free of degenerate solution. IEEE Trans. Signal Process. 55 (5), 1803–1814. https://doi.org/10.1109/TSP.2006.889983.

Long, Q., Bhinge, S., Calhoun, V.D., Adali, T., 2020. Independent vector analysis for common subspace analysis: Application to multi-subject fMRI data yields meaningful subgroups of schizophrenia. NeuroImage, 116872.

Ma, S., Phlypo, R., Calhoun, V.D., Adalı, T., 2013. Capturing group variability using IVA: a simulation study and graph-theoretical analysis. In: 2013 IEEE International Conference on Acoustics, Speech and Signal Processing (ICASSP). Vancouver, Canada.

Ma, S., Calhoun, V.D., Phlypo, R., Adalı, T., 2014. Dynamic changes of spatial functional network connectivity in healthy individuals and schizophrenia patients using independent vector analysis. NeuroImage 90, 196–206.

Michael, A., Anderson, M., Miller, R., Adalı, T., Calhoun, V.D., 2014. Preserving subject variability in group fMRI analysis: Performance evaluation of GICA versus IVA. Front. Syst. Neurosci. 8, 106–123.

Park, B.-y., Moon, T., Park, H., 2018. Dynamic functional connectivity analysis reveals improved association between brain networks and eating behaviors compared to static analysis. Behav. Brain Res. 337, 114–121.

Rashid, B., Damaraju, E., Pearlson, G.D., Calhoun, V.D., 2014. Dynamic connectivity states estimated from resting fMRI identify differences among schizophrenia, bipolar disorder, and healthy control subjects. Front. Hum. Neurosci. 8, 897.

Rubinov, M., Sporns, O., 2010. Complex network measures of brain connectivity: Uses and interpretations. NeuroImage 52 (3), 1059–1069.

Savva, A.D., Kassinopoulos, M., Smyrnis, N., Matsopoulos, G.K., Mitsis, G.D., 2020. Effects of motion related outliers in dynamic functional connectivity using the sliding window method. J. Neurosci. Methods 330, 108519.

Scott, A., Courtney, W., Wood, D., De la Garza, R., Lane, S., Wang, R., King, M., Roberts, J., Turner, J.A., Calhoun, V.D., 2011. COINS: An innovative informatics and neuroimaging tool suite built for large heterogeneous datasets. Front. Neuroinform. 5, 33.

Shin, J., Ahn, S., Hu, X., 2013. Correction for the T1 effect incorporating flip angle estimated by Kalman filter in cardiac-gated functional MRI. Magn. Reson. Med. 70 (6), 1626–1633.

Sorber, L., Van Barel, M., De Lathauwer, L., 2015. Structured data fusion. IEEE J. Sel. Top. Signal Process. 9 (4), 586–600.

Stegeman, A., 2020. Comparing Independent Component Analysis and the Parafac Model for Artificial Multi-subject fMRI Data, Unpublished Technical Report. Univ. of Groeningen.
Telesford, Q.K., Burdette, J.H., Laurienti, P.J., 2020. An exploration of graph metric reproducibility in complex brain networks. Front. Neurosci. 7.
Vergara, V.M., Salman, M., Abrol, A., Espinoza, F.A., Calhoun, V.D., 2020. Determining the number of states in dynamic functional connectivity using cluster validity indexes. J. Neurosci. Methods, 108651.
Wang, L., Yu, C., Chen, H., Qin, W., He, Y., Fan, F., Zhang, Y., Wang, M., Li, K., Zang, Y., Woodward, T.S., Zhu, C., 2010. Dynamic functional reorganization of the motor execution network after stroke. Brain 133 (4), 1224–1238.
Weber, S., Johnsen, E., Kroken, R.A., Løberg, E.-M., Kandilarova, S., Stoyanov, D., Kompus, K., Hugdahl, K., 2020. Dynamic functional connectivity patterns in schizophrenia and the relationship with hallucinations. Front. Psychiatry 11, 227.
Zhang, W., Li, S., Wang, X., Gong, Y., Yao, L., Xiao, Y., Liu, J., Keedy, S.K., Gong, Q., Sweeney, J.A., et al., 2018. Abnormal dynamic functional connectivity between speech and auditory areas in schizophrenia patients with auditory hallucinations. Neuroimage Clin. 19, 918–924.
Zhi, D., Ma, X., Lv, L., Ke, Q., Yang, Y., Yang, X., Pan, M., Qi, S., Jiang, R., Du, Y., et al., 2018. Abnormal Dynamic Functional Network Connectivity and Graph Theoretical Analysis in Major Depressive Disorder, pp. 558–561.